



DØ Note 5935-CONF

## Combined Upper Limits on MSSM Higgs-Boson Production with up to $2.6 \text{ fb}^{-1}$ of Data at DØ

The DØ Collaboration  
URL <http://www-d0.fnal.gov>

Results are presented on the search for a neutral MSSM Higgs boson, combining the  $h \rightarrow \tau\tau$ ,  $bh \rightarrow b\tau\tau$ , and  $bh \rightarrow bb\bar{b}$  final states, using  $2.2 \text{ fb}^{-1}$ ,  $1.2 \text{ fb}^{-1}$  and  $2.6 \text{ fb}^{-1}$ , respectively, of integrated luminosity collected at the DØ experiment. Data were collected in  $p\bar{p}$  collisions at a centre of mass energy of 1.96 TeV during RunII of the Tevatron. Limits for Higgs masses in the range  $100 < M_A < 220 \text{ GeV}$  are set at the 95% confidence level in the  $\tan\beta$ - $M_A$  plane in four different benchmark scenarios within the framework of the MSSM.

*Preliminary Results*

## I. INTRODUCTION

Supersymmetry (SUSY) as an extension to the Standard Model (SM) provides a natural solution to the hierarchy problem as well as potentially providing a dark matter candidate and GUT-scale unification. In its simplest form the Minimal Supersymmetry Standard Model [1] (MSSM) requires the introduction of two Higgs doublet fields, predicting the existence of five physical Higgs bosons after symmetry breaking. Three of these are neutral ( $h$ ,  $H$ , and  $A$ ) and two are charged  $H^\pm$ . The ratio of the vacuum expectation values of the two doublets is denoted by  $\tan\beta$ . At leading order the Higgs sector can be described by two parameters chosen here to be  $M_A$  (the mass of the  $A$ ) and  $\tan\beta$ . The couplings of the  $A$  to the charged leptons and the down-type quarks are enhanced by a factor of  $\tan\beta$ , while the coupling to neutrinos and up-type quarks are suppressed by a similar factor. At large values of  $\tan\beta$  two of the three neutral bosons have approximately the same mass and couplings thus are effectively degenerate. This contributes an additional factor of two enhancement in the cross section. Thus the overall enhancement at leading-order scales approximately as  $2 \times \tan^2 \beta$ . For low  $M_A$ , and high  $\tan\beta$  the Tevatron can set strong limits within a number of benchmark scenarios (described below) in the MSSM that complement the searches carried out by the LEP experiments [2].

## II. ANALYSIS SUMMARY

The DØ detector is described in detail elsewhere [3]. The searches combined in this analysis are described in detail in [4–8]. Though not included in this combination, searches in these channels using around a third of the integrated luminosity from Run IIa can be found in [9–11]. Results of similar searches from CDF in Run II at the Tevatron are found in [12–14].

Inputs are taken from searches from three distinct signatures: an inclusive search in the  $h \rightarrow \tau\tau$  channel, and two exclusive searches looking for Higgs production in association with a  $b$ -quark:  $bh \rightarrow b\tau\tau$  and  $bh \rightarrow bb\bar{b}$  using up to  $2.6 \text{ fb}^{-1}$  of integrated luminosity collected during Run IIa and Run IIb at the Tevatron. The breakdown of luminosity collected in each channel is given in Table I.

| Channel                                      | Integrated Luminosity / $\text{fb}^{-1}$ |         | Final Variable  |
|--|--|---------|-----------------|
|  | Run IIa                                  | Run IIb |                 |
| $h \rightarrow \tau_e \tau_{\text{had}}$     | 1.0                                      | -       | visible mass    |
| $h \rightarrow \tau_\mu \tau_{\text{had}}$   | 1.0                                      | 1.2     | visible mass    |
| $h \rightarrow \tau_e \tau_\mu$              | 1.0                                      | -       | visible mass    |
| $bh \rightarrow b\tau_\mu \tau_{\text{had}}$ | -  | 1.2     | 1D-discriminant |
| $bh \rightarrow bb\bar{b}$                   | 1.0                                      | 1.6     | $M_{bb}$        |

TABLE I: Integrated luminosity collected for each final state signature. The last column shows the final variable used for the limit calculation. In the  $h \rightarrow \tau\tau$  channels this variable is the visible mass,  $M_{\text{vis}} = \sqrt{P_{\tau_1} + P_{\tau_2} + \cancel{P}_T}$ , where  $P_{\tau_{1/2}}$  are the four-vectors of the visible products of the two tau decays and  $\cancel{P}_T = (\cancel{E}_T, \cancel{E}_x, \cancel{E}_y, 0)$ , in  $bh \rightarrow b\tau\tau$  it is a one dimensional combination of a neural network and a likelihood discriminant and in the  $bh \rightarrow bb\bar{b}$  channel the invariant di-jet mass is used.

The tau channels are split into channels based on the final state decays of the  $\tau$ -leptons:  $\tau_e \tau_{\text{had}}$ ,  $\tau_\mu \tau_{\text{had}}$ , and  $\tau_e \tau_\mu$ , where  $\tau_e$ ,  $\tau_\mu$  and  $\tau_{\text{had}}$  denote tau decays to an electron, muon or hadrons respectively. Further subdivision of the channels is made based on the characteristics of the  $\tau_{\text{had}}$  decay. The  $bh \rightarrow bb\bar{b}$  analysis is divided into three channels with 3, 4 or 5 jets in the final state. This gives a total of 19 sub-channels combined in the process of setting limits.

### A. Object Identification

Electrons are identified through their characteristic energy deposits in the calorimeters. Clusters of energy reconstructed in the calorimeter are required to be isolated both in the calorimeter and in the tracking detectors. These must have a single spatially matched track whose momentum divided by the cluster energy must be close to one. Muons are identified by matching charged tracks in the central tracking detectors with hits in the muon detectors. Muon candidates are also required to be isolated in both the central tracking detectors and in the calorimeter. The hadronic decays of the  $\tau$  are split into three categories:  $\tau$ -types 1 and 2 are 1-prong candidates with energy either only in the hadron calorimeter ( $\pi^\pm$  like) or in both the electromagnetic and hadron calorimeters ( $\rho^\pm$  like) respectively;  $\tau$ -type 3 is a 3-prong candidate with an invariant mass below 1.7 GeV and matching energy deposits in the calorimeters. A neural network (NN) is trained for each type to separate hadronic tau decays from jets using Monte-Carlo

(MC)  $Z \rightarrow \tau\tau$  as the signal and multi-jet events taken from data as the background. An additional NN is trained on electron MC events and is employed to reduce backgrounds from electrons faking type 2 taus.

A mid-point cone algorithm is used to reconstruct hadronic jets from energy deposits in the calorimeter[15]. Jet reconstruction and energy scale determination are described in detail in [16].  $b$ -jet candidates must pass a set of quality criteria, and must have two or more charged tracks within a cone about the jet axis of radius:  $\Delta R = \sqrt{(\Delta\eta)^2 + (\Delta\phi)^2} < 0.5$ .  $b$ -jets are then identified using a neural network (NN) algorithm which takes as inputs lifetime information derived from track impact parameters and secondary vertices [17].

## B. Signal, Backgrounds and Event Selection

The signal acceptance is determined using the leading-order (LO) MC generator PYTHIA [18], with CTEQ6L [19] parton sets. Detector response is modeled using GEANT [23] based simulations and additional weights are applied to correct for the trigger efficiency. Within the MSSM the dominant production processes for  $h \rightarrow \tau\tau$  are  $gg \rightarrow h \rightarrow \tau\tau$  and  $bb \rightarrow h \rightarrow \tau\tau$ . The signal acceptance is similar for both these processes and so only the  $gg \rightarrow h$  contribution is considered (though both are included in determining the final signal normalisation discussed below). The 5-flavor scheme [20] ( $gb \rightarrow hb$ ) is used for the associated production channels and TAUOLA[21] is used to simulate the final state tau decays. Additionally, corrections for next-to-leading order effects on the Higgs production kinematics in the  $bh \rightarrow bb\bar{b}$  channels are computed using MCFM [20] and applied as weights as a function of  $p_T$  and  $\eta$  of the spectator  $b$ -jet.

Most Standard Model backgrounds have been generated with PYTHIA:  $Z/\gamma^* \rightarrow l^+l^-$ ,  $W \rightarrow l\nu$ , di-boson production,  $t\bar{t}$  (COMPHEP + PYTHIA)[22]. MC samples for  $W$  and  $Z$  bosons produced in associated with jets have been produced with ALPGEN [24] matched to PYTHIA for hadronization. The normalisation of the di-boson and  $t\bar{t}$  samples is made to next-to-LO (NLO) while the  $Z/\gamma^*$  samples are normalised to next-to-NLO (NNLO).

### 1. $h \rightarrow \tau\tau$

Events are selected online using inclusive electron and muon triggers ( $\tau_e\tau_{\text{had}}$   $\tau_\mu\tau_{\text{had}}$ ) and electron + muon triggers ( $\tau_e\tau_\mu$ ). After offline reconstruction, candidate events must contain two isolated opposite charged final state leptons ( $e, \mu, \tau$ ) within the fiducial region:  $|\eta_{e/\tau}| < 2.5$ ,  $|\eta_\mu| < 2.0$ . Additionally electron candidates must not lie close to the boundary region between the central and endcap cryostats,  $1.1 < |\eta_e| < 1.5$ . In the  $\tau_e\tau_{\text{had}}$  and  $\tau_\mu\tau_{\text{had}}$  channels the electron or muon are required to be isolated and have a transverse momentum,  $p_T > 15$  GeV. 1-prong hadronic tau candidates are accepted with  $p_T > 16.5$  GeV and 3-prong candidates are required to have  $p_T > 22$  GeV. Additional cuts on the relative directions of the taus and the missing transverse energy in the event,  $\cancel{E}_T$  - calculated from the position and energy of cells in the calorimeter, are imposed for the  $\tau_e\tau_{\text{had}}$  final state. For both the  $\tau_e\tau_{\text{had}}$  and  $\tau_\mu\tau_{\text{had}}$  final states requirements are made on the transverse mass,  $M_T = \sqrt{2p_T^{e/\mu} \cancel{E}_T(1 - \cos\Delta\phi)}$ , where  $\Delta\phi$  is the azimuthal angle between the electron or muon and the  $\cancel{E}_T$ . These two cuts serve to suppress background contributions from  $W$ +jets production. In the  $\tau_e\tau_\mu$  channel events containing one electron and one muon are selected, where:  $p_T^\mu > 10$  GeV and  $p_T^e > 12$  GeV and the invariant mass of the electron-muon pair exceeds 20 GeV and  $|E_T^e| + |p_T^\mu| + |\cancel{E}_T| > 65$  GeV. Further cuts are made on the minimal transverse mass,  $M_T^{\text{min}}$  - the smallest of  $M_T^{l=e}$  and  $M_T^{l=\mu}$ , and the angle between the softest lepton and the  $\cancel{E}_T$ .

Leading SM and instrumental sources of background in  $h \rightarrow \tau\tau$  are:  $Z/\gamma^* \rightarrow \tau\tau$ , multi-jet,  $W \rightarrow e\nu, \mu\nu, \tau\nu$ ,  $Z \rightarrow \mu\mu$ ,  $Z \rightarrow ee$ , di-boson ( $WW, WZ, ZZ, W\gamma, Z\gamma$ ), and  $t\bar{t}$ -pair production. The multi-jet contribution is estimated from data using either  $\tau_e\tau_{\text{had}}$  candidate events where the electron and  $\tau$  have the same charge or using inverted lepton selection criteria ( $\tau_\mu\tau_{\text{had}}$  and  $\tau_e\tau_\mu$  channels). The normalisation of the  $W$  production backgrounds is estimated from a data sample dominated by  $W$ +jet events. The visible mass distribution is used in the setting of limits.

### 2. $bh \rightarrow b\tau\tau$

Data events in this channel are selected online using high  $p_T$  single muon and special muon + hadronic tau triggers. Events are required to include one isolated muon with  $p_T > 12$  GeV,  $|\eta| < 2.0$ , with a matching central track. Events with more than one muon are rejected to suppress backgrounds from  $Z \rightarrow \mu\mu$ . 1-prong tau candidates must have,  $E_T > 10$  GeV,  $p_T^{\text{trk}} > 5(\text{type1}), 7(\text{type2})$  GeV. 3-prong tau candidates are required to meet slightly tighter criteria:  $E_T > 15$  GeV, with at least 1 track with  $p_T > 5$  GeV and sum of track  $p_T^{\text{trk}} > 10$  GeV. Events must then have at

least one good  $b$ -tagged jet isolated from the muon and tau with  $p_T > 15$  GeV,  $|\eta| < 2.5$ , and  $|\eta_{\text{det}}| < 2.5$ , where  $\eta_{\text{det}}$  is the jet pseudorapidity measured with respect to the detector centre rather than the primary vertex.

Dominant backgrounds arise from multi-jet production, top pair production, and  $Z \rightarrow \tau\tau$  produced with heavy flavour jets. Additional backgrounds making small contributions come from processes such as  $Z \rightarrow \tau\tau$  + light jets,  $Z \rightarrow \mu\mu$ ,  $W$ +jets, single top-quark production and diboson production. The multi-jet background is estimated from data using inverted lepton and tau identification cuts and no  $b$ -tagging to select a multi-jet rich background sample. The multi-jet content of this sample is then estimated from comparing the number of events with  $\mu$  and  $\tau$  charge the same with the number of events where they are oppositely charged. Then the average of two complimentary methods of estimating the background from this sample is used. The first method makes use of a measurement of the  $b$ -tagging probability and the second a measurement of the muon isolation and tau mis-identification rates in order to extrapolate from the background rich sample into the signal region. A neural network and a likelihood are trained to reject  $t\bar{t}$  and multi-jet backgrounds respectively. The output of these are combined into a single discriminant whose distribution is used as the input to the limit setting.

### 3. $bh \rightarrow b\bar{b}$

Dedicated triggers designed to select events with at least three jets are used in this analysis. At least three and at most five jets within the fiducial region ( $|\eta| < 2.5$ ,  $p_T > 20$  GeV) are required to pass tight NN- $b$ -tagging cuts. The per  $b$ -jet tagging efficiency is around 50% with a light-jet mis-identification rate at the level of 0.5-1.5%. Additionally, the two leading jets must have  $p_T > 25$  GeV. Signal sensitivity is further enhanced by breaking the sample into three channels containing exactly 3, 4 and 5 fiducial jets in the final state. A likelihood technique using a set of kinematic variables is employed to further enhance the selection of signal over background. Two separate likelihoods are used: one for the mass region  $90 \leq M_A < 140$  GeV and the other for  $140 \leq M_A < 260$  GeV. Heavy flavour multi-jet backgrounds dominate and are estimated using a data driven method by applying a 2D-transformation (in  $M_{b\bar{b}}$  and  $\mathcal{D}$  the value of the likelihood discriminant) to a data sample containing  $\geq 2$   $b$ -tagged jets, derived from the ratio of MC events containing  $\geq 3$   $b$ -tagged jets to those containing  $\geq 2$   $b$ -tagged jets. For the setting of limits the invariant mass distribution of the two mass pairings constructed from the leading and next-to-leading  $b$ -tagged jets and the leading and next-to-next-to-leading  $b$ -tagged jets are used. The  $M_{b\bar{b}}$  invariant mass resolution in the  $bh \rightarrow b\bar{b}$  channels is sufficiently narrow that the finite width of the Higgs becomes important and degrades the limit. The width effects are simulated by generating a narrow SM-like Higgs over a range of masses and mixing them weighted by an appropriate relativistic Breit-Wigner distribution.

## C. Event distributions

Table II shows the expected number of background and observed events in data as well as the signal efficiency for  $M_A = 160$  GeV for the  $h \rightarrow \tau\tau$  and  $bh \rightarrow b\tau\tau$  channels, only statistical uncertainties are shown. Table III shows the expected number of data events and the signal efficiency for  $M_A = 160$  GeV for a narrow SM-like Higgs in the  $bh \rightarrow b\bar{b}$  channels.

| Source                                    | Run IIa<br>$h \rightarrow \tau\tau$ |                           |                             | Run IIb   |   |
|---|-------------------------------------|---------------------------|-----------------------------|---|---|
|   | $\tau_e\tau_\mu$                    | $\tau_e\tau_{\text{had}}$ | $\tau_\mu\tau_{\text{had}}$ | $bh \rightarrow b\tau\tau$<br>$\tau_\mu\tau_{\text{had}}$ | $h \rightarrow \tau\tau$<br>$\tau_\mu\tau_{\text{had}}$ |
| $Z \rightarrow ee / Z \rightarrow \mu\mu$ | $10.4 \pm 0.9$                      | $31 \pm 2$                | $19 \pm 1$                  | $0.35 \pm 0.02$   | $48 \pm 6$  |
| $Z \rightarrow \tau\tau$                  | $212 \pm 3.0$                       | $581 \pm 5$               | $1130 \pm 7$                | $1.56 \pm 0.02$   | $1030 \pm 32$   |
| $W \rightarrow l\nu$                      | $9.3 \pm 2.3$                       | $42 \pm 5$                | $32 \pm 4$                  | (included in multi-jet)                                   |   |
| diboson + $t\bar{t}$                      | $6.1 \pm 0.1$                       | $3.0 \pm 0.1$             | $7.0 \pm 0.4$               | $2.13 \pm 0.21$   | $8.7 \pm 2.6$   |
| Multi-jet                                 | $8.6 \pm 0.8$                       | $332 \pm 20$              | $86 \pm 4$                  | $6.01 \pm 0.75$   | $96 \pm 9$  |
| Background Total                          | $266 \pm 4$                         | $989 \pm 22$              | $1274 \pm 9$                | $13.9 \pm 0.8$  | $1189 \pm 34$   |
| Data                                      | 274                                 | 1034                      | 1231                        | 20  | 1109  |
| Signal Efficiency /%                      | $0.57 \pm 0.03$                     | $1.04 \pm 0.03$           | $1.46 \pm 0.04$             | $0.42 \pm 0.13$   | $1.1 \pm 0.3$   |

TABLE II: Estimated background, observed data events and signal efficiency for  $M_A = 160$  GeV, for  $h \rightarrow \tau\tau$  and  $bh \rightarrow b\tau\tau$  analyses. The errors shown are statistical only.

In setting the limits, events from regions of phase-space with a similar ratio of expected signal (S) to background (B) can be combined without loss of sensitivity. Thus a useful way to visualize the comparison of expected backgrounds

| No. Jets             | Run IIa   |      |     | Run IIb   |      |     |
|----------------------|-----------|------|-----|-----------|------|-----|
|                      | 3         | 4    | 5   | 3         | 4    | 5   |
| Data                 | 3431      | 2571 | 676 | 4326      | 3277 | 852 |
| Signal Efficiency /% | 2.1 ± 0.1 |      |     | 1.4 ± 0.1 |      |     |

TABLE III: Number of observed events and estimated signal efficiency at  $M_A = 160$  GeV for a SM-like Higgs for the  $bh \rightarrow b\bar{b}$  analyses. The errors shown are statistical only.

and the observed data is to show the event distributions binned in this ratio S/B. For the channels combined in this note these distributions are shown in Figure 1 for two mass points:  $M_A=130$  and 220 GeV for  $\tan\beta=60$ . These plots do not include the systematic uncertainties and generally good agreement is observed between the background model and the data.

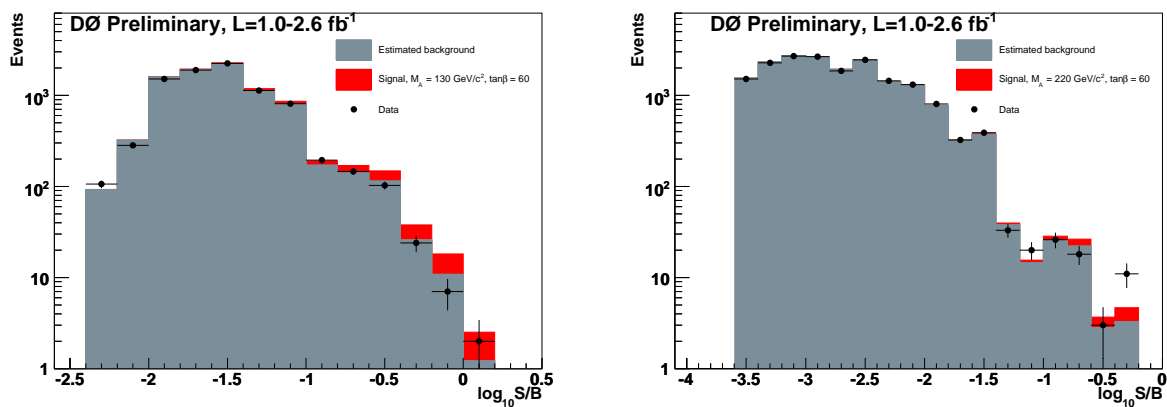


FIG. 1: Events binned by the ratio of expected signal (S) to expected background (B) for  $\tan\beta=60$  in the maximal mixing scenario with positive  $\mu$  parameter for  $M_A=130$  GeV (left), and  $M_A=220$  GeV (right). The points show the observed data with statistical errors only.

### III. COMBINATION

Limits are set using the *modified frequentist* (or  $CL_S$ ) technique [25]. The test statistic is a negative log-likelihood ratio:

$$LLR = -2 \ln \frac{p(\text{data}|H_1)}{p(\text{data}|H_0)}, \quad (1)$$

where  $H_1$  is the test (background + signal) hypothesis,  $H_0$  is the null (background only) hypothesis and  $p$  are Poisson probabilities for obtaining the observed number of events under each hypothesis.  $CL_S$  is defined by the ratio:  $CL_S = CL_{s+b}/CL_b$  where,  $CL_{s+b}$  and  $CL_b$  are the confidence levels for the test and null hypothesis respectively. These confidence levels are estimated by integrating the probability density functions for the test statistic under the two hypotheses generated using simulated pseudo-experiments. Systematic uncertainties on the signal and background are introduced using Gaussian sampling. A profile likelihood technique[26] is used to reduce the impact of the systematics on the final limits.

For the individual analyses limits have generally been set in a model independent way on the cross section  $\times$  branching ratio for the final state being considered. When combining these channels together this is no longer possible since the relative weights - ie their cross section  $\times$  branching ratios up to a global scale factor - vary depending on the model being considered. For the purposes of this combination four benchmark scenarios have been used and the normalisations for the  $h \rightarrow \tau\tau$  and  $bh \rightarrow b\tau\tau$  channels are taken from FEYNHIGGS[27]. For the  $bh \rightarrow b\bar{b}$  channels they are normalised to the SM cross section from MCFM and then scaled to the appropriate MSSM cross section  $\times$  branching ratio making use of FEYNHIGGS. In this preliminary results theoretical uncertainties have only been included on the

signal acceptance. Those affecting the overall normalisation of the signals have not yet been introduced into the limit setting procedure. Though the  $h \rightarrow \tau\tau$  and  $bh \rightarrow b\tau\tau$  channels are not strictly orthogonal the overlap is small enough to have no significant effect on the combination. In calculating the confidence limits, signal samples within each scenario for each of the 19 sub-channel inputs are prepared on a grid spanning the  $\tan\beta - M_A$  plane and for each mass hypothesis the limit is evaluated by interpolating between the two grid points spanning  $CL_S = 0.05$ .

#### IV. SYSTEMATIC UNCERTAINTIES

Numerous sources introduce systematic uncertainties into the numbers of background and signal events expected for each input channel. Some uncertainties are applied as *shape systematics* which correlate a varying uncertainty across each bin of the associated input distributions. This contrasts with a *flat systematic* which introduces a constant uncertainty correlated across each bin of the input distribution. Uncertainties arising from similar or identical sources, for example in the use of common measurements of lepton identification efficiencies, are assumed to be 100% correlated across channels as appropriate. Table IV summarises the list of dominant systematics by channel, shows the correlations between them and indicates the approximate size of each systematic on the number of signal and background events.

The uncertainty on the integrated luminosity is 6.1% and is correlated across all channels. Uncertainties on lepton-identification efficiencies (4-8%) and energy scale (3%) are generally correlated across channels by lepton type within an epoch (Run IIa or Run IIb). The uncertainty associated with the measurement of trigger efficiencies (3-4%) is correlated across channels sharing the same triggers. Further significant sources of systematic uncertainty are identified: parton density functions (PDF) (4%),  $Z/\gamma^*$  production (5%), and  $W$ -boson background normalisation (6-15%). The measurement of the normalisation of the multi-jet backgrounds (4-47%) is data driven and specific to each channel - though correlated across sub-channels. In the  $bh \rightarrow b\tau\tau$  channels there are particularly large uncertainties arising from the modelling of  $W$  and  $Z$  boson production associated with a  $b$ - or  $c$ -jet (50%).

In the  $bh \rightarrow bb\bar{b}$  analyses only variations in the shape of the background distribution are considered - the overall background normalisation is allowed to float in the fitting procedure (independently for the test and null hypotheses) during evaluation of the limits. The dominant source of uncertainty arises from the modeling of the composition in the MC used to derive the templates used in constructing the background model. Additional contributions come from:  $b$ -jet resolution and  $b$ -tagging efficiency, modeling of the kinematics of the different components of the background (assessed using a sideband control sample) and finally the bias induced by the variation in the trigger turn-on for triple and double  $b$ -tagged samples. These are considered correlated across the three channels (3-,4- and 5-jet) within each data taking epoch, with only the  $b$ -jet resolution systematic being correlated across epochs. Though some of these sources of systematic uncertainties are conceivably connected with similar sources in the  $bh \rightarrow b\tau\tau$  channel the method of floating the overall normalisation uncertainty in the limit fits is assumed to remove much of any correlation on the background uncertainties. The signal uncertainties in these two channels are dominated by uncorrelated contributions.

#### V. COMBINED RESULTS AND INTERPRETATION WITH THE MSSM

Tables V, VI, VII, and VIII give the observed and median expected 95% confidence limits on  $\tan\beta$  for the tested mass hypotheses for the four different benchmark scenarios considered [28]. This is shown graphically in Figure 2. The four scenarios considered are defined in terms of:  $M_{SUSY}$ , the mass scale of squarks,  $\mu$ , the Higgs sector bilinear coupling,  $M_2$ , the gaugino mass term,  $X_t$ , the mixing parameter,  $A_t$ , the trilinear coupling of the stop sector,  $A_b$ , the trilinear coupling of the sbottom sector and  $m_{\tilde{g}}$  the gluino mass term. The maximal-mixing,  $m_h^{max}$ , scenario is defined as:

$$\begin{aligned} M_{SUSY} &= 1\text{TeV}, \mu = 200\text{GeV}, M_2 = 200\text{GeV}, \\ X_t &= 2M_{SUSY} \\ A_b &= A_t, m_{\tilde{g}} = 0.8M_{SUSY}. \end{aligned}$$

and the no-mixing scenario - with vanishing mixing in the stop sector and a higher SUSY mass scale to avoid the LEP Higgs bounds:

| Source                                   | RunIIa                   |                           |                             |   | RunIIb                      |                             |                            | Signal<br>/% | Background<br>/% |
|--|--------------------------|---------------------------|-----------------------------|---|-----------------------------|-----------------------------|----------------------------|--------------|------------------|
|  | $h \rightarrow \tau\tau$ |                           | $bh \rightarrow bb\bar{b}$  |   | $h \rightarrow \tau\tau$    | $bh \rightarrow b\tau\tau$  | $bh \rightarrow bb\bar{b}$ |              |                  |
|  | $\tau_e\tau_\mu$         | $\tau_e\tau_{\text{had}}$ | $\tau_\mu\tau_{\text{had}}$ |   | $\tau_\mu\tau_{\text{had}}$ | $\tau_\mu\tau_{\text{had}}$ |                            |              |                  |
| Luminosity                               | ×                        | ×                         | ×                           | × | ×                           | ×                           | ×                          | 6.1          | 6.1              |
| PDF                                      | ×                        | ×                         | ×                           | - | ×                           | ×                           | -                          | 4            | -                |
| EM-Trigger                               | -                        | ×                         | -                           | - | -                           | -                           | -                          | 3-5          | 3-5              |
| Muon Trigger                             | -                        | -                         | ×                           | - | ×                           | ×                           | -                          | 3-5          | 3-5              |
| EM-Muon Trigger                          | ×                        | -                         | -                           | - | -                           | -                           | -                          | 3-4          | 3-4              |
| EM-ID                                    | ×                        | ×                         | -                           | - | -                           | -                           | -                          | 3-8          | 3-8              |
| Muon-ID                                  | ×                        | -                         | ×                           | - | ×                           | ×                           | -                          | 4-8          | 4-8              |
| $\tau_{\text{had}}$ -ID                  | -                        | *                         | *                           | - | *                           | *                           | -                          | 4-10         | 4-10             |
| $\tau_{\text{had}}$ -energy scale (IIa)  | -                        | *                         | *                           | - | -                           | -                           | -                          | 2-4          | 2-4              |
| $\tau_{\text{had}}$ -energy scale (IIb)  | -                        | -                         | -                           | - | *                           | *                           | -                          | 2-4          | 2-4              |
| $\tau_{\text{had}}$ track reconstruction | -                        | ×                         | ×                           | - | ×                           | ×                           | -                          | 1-2          | 1-2              |
| $\tau_\mu$ track reconstruction          | -                        | -                         | ×                           | - | ×                           | ×                           | -                          | 1-2          | 1-2              |
| b-tagging                                | -                        | -                         | -                           | † | -                           | †                           | †                          | 6-10         | 1-2              |
| Jet energy scale and modelling           | ×                        | ×                         | ×                           | - | ×                           | ×                           | -                          | 0.1-6        | 0.1-6            |
| $W \rightarrow \mu\nu + \text{jets}$     | ×                        | -                         | ×                           | - | ×                           | ×                           | -                          | -            | 6-15             |
| $Z \rightarrow ee$                       | -                        | ×                         | -                           | - | -                           | -                           | -                          | -            | 5-13             |
| Other MC background                      | ×                        | ×                         | ×                           | - | ×                           | -                           | -                          | -            | 5                |
| Heavy flavour MC                         | -                        | -                         | -                           | - | -                           | ×                           | -                          | -            | 50               |
| $bbb$ and $bbj$ modelling                | -                        | -                         | -                           | † | -                           | -                           | †                          | -            | s                |
| Multi-jet backgrounds                    | -                        | †                         | †                           | † | †                           | †                           | †                          | -            | 4-47             |

TABLE IV: List of dominant systematics and their correlations.  $\times$  denotes a correlation across channels and sub-channels (such as  $\tau$ -type),  $*$  denotes a correlation across channels but only for the same  $\tau$ -type,  $\dagger$  denotes a correlation across sub-channels but not between channels. The last two columns give an approximate size of the uncertainty on the number of signal and background events. An  $s$  denotes pure shape systematics in the  $bh \rightarrow bb\bar{b}$  analysis.

$$M_{\text{SUSY}} = 2\text{TeV}, \mu = 200\text{GeV}, M_2 = 200\text{GeV},$$

$$X_t = 0, A_b = A_t, m_{\bar{g}} = 0.8M_{\text{SUSY}}.$$

Four scenarios are constructed from these two by the consideration of both + and - signs for  $\mu$ .

Differences are seen in the limits depending sign of  $\mu$ . These difference arise where radiative corrections to the  $h/H/Ab\bar{b}$  coupling have a significant effect on the production cross section, branching fraction and width for  $bh \rightarrow bb\bar{b}$ . Though as  $\tan\beta$  gets lower this variation should decrease. These effects are less significant in the no-mixing scenario. Limits have been set on  $\tan\beta$  as low as 30-35 at the most sensitive mass point - 130 GeV - rising to 70-100 (depending on scenario) at 220 GeV and with the exception of at the high end of the mass scale the observed limits are within the  $1\sigma$  band around the *background only* expectation. This result significantly extends the previous combination reported in [10] with over 7 times the integrated luminosity and sets the most stringent limits to date on neutral MSSM Higgs boson production at hadron colliders.

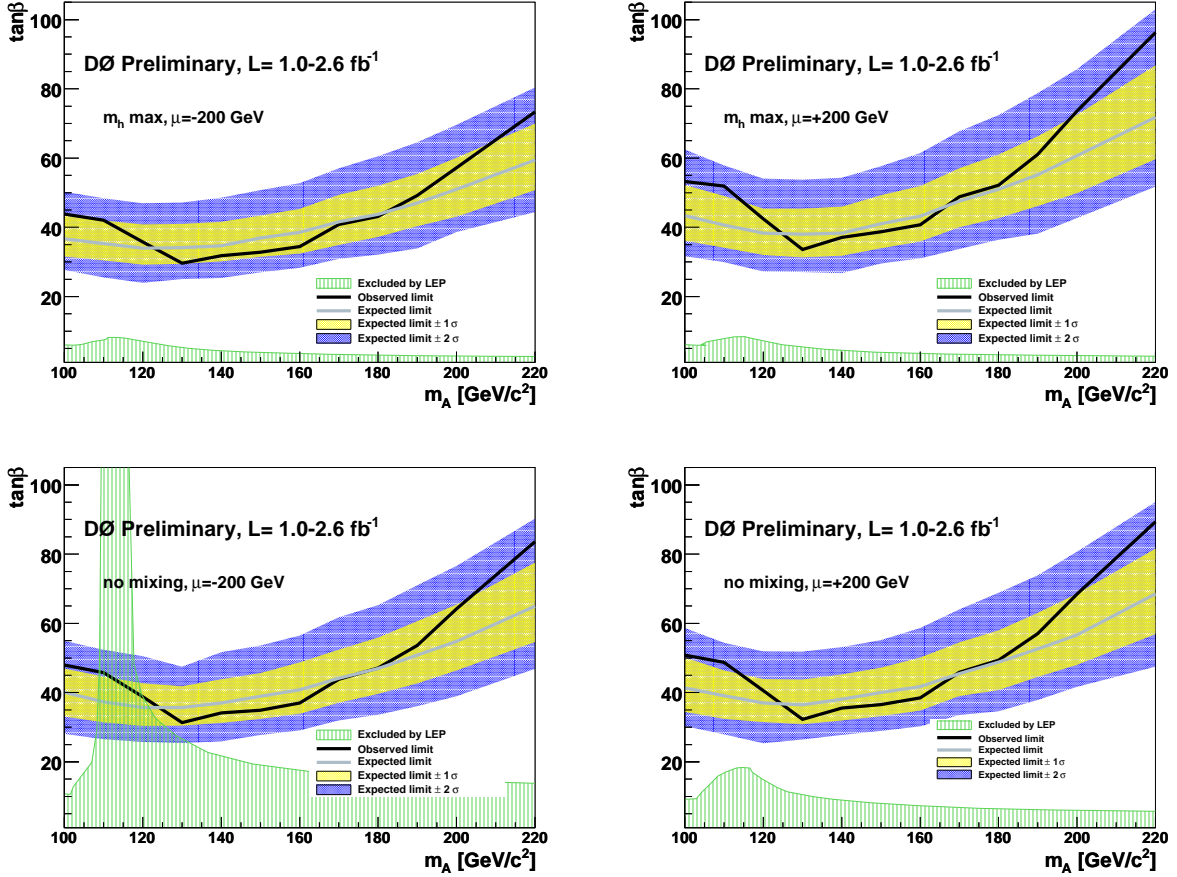


FIG. 2: 95% Confidence limits in the  $\tan\beta$ - $M_A$  plane for the 4 benchmark scenarios: maximal mixing (top) and no mixing (bottom) for  $\mu < 0$  (left) and  $\mu > 0$  (right). The dark shaded region shows the observed limit, the solid line the expected limit and the shaded light-green area shows the limits from LEP.

| Mass / GeV | Observed limit | Expected Limits |            |        |            |            |
|------------|----------------|-----------------|------------|--------|------------|------------|
|            |                | $-2\sigma$      | $-1\sigma$ | Median | $+1\sigma$ | $+2\sigma$ |
| 100        | 53             | 32              | 36         | 43     | 52         | 62         |
| 110        | 52             | 30              | 34         | 41     | 50         | 58         |
| 120        | 42             | 27              | 32         | 38     | 45         | 54         |
| 130        | 34             | 27              | 31         | 38     | 45         | 54         |
| 140        | 37             | 27              | 32         | 38     | 46         | 54         |
| 150        | 39             | 30              | 34         | 41     | 49         | 58         |
| 160        | 41             | 31              | 36         | 43     | 52         | 61         |
| 170        | 49             | 34              | 40         | 48     | 57         | 68         |
| 180        | 52             | 36              | 43         | 51     | 61         | 72         |
| 190        | 61             | 38              | 46         | 55     | 66         | 79         |
| 200        | 74             | 43              | 50         | 61     | 72         | 86         |
| 220        | 96             | 52              | 60         | 72     | 87         | 103        |

TABLE V: Limits on  $\tan\beta$  for each Higgs mass hypothesis in the maximal mixing and positive  $\mu$  scenario. For the expected limit the  $\pm 1$  and  $2\sigma$  limits are also given.

| Mass / GeV | Observed<br>limit | Expected Limits |            |        |            |            |
|------------|-------------------|-----------------|------------|--------|------------|------------|
|            |                   | $-2\sigma$      | $-1\sigma$ | Median | $+1\sigma$ | $+2\sigma$ |
| 100        | 44                | 28              | 32         | 37     | 43         | 50         |
| 110        | 42                | 25              | 31         | 35     | 42         | 48         |
| 120        | 36                | 24              | 29         | 34     | 41         | 47         |
| 130        | 30                | 25              | 29         | 34     | 41         | 47         |
| 140        | 32                | 25              | 30         | 35     | 42         | 49         |
| 150        | 33                | 27              | 32         | 37     | 43         | 51         |
| 160        | 34                | 28              | 32         | 39     | 45         | 53         |
| 170        | 41                | 31              | 35         | 42     | 49         | 57         |
| 180        | 43                | 32              | 37         | 44     | 52         | 61         |
| 190        | 49                | 34              | 40         | 47     | 55         | 65         |
| 200        | 57                | 39              | 43         | 51     | 60         | 70         |
| 220        | 73                | 44              | 51         | 59     | 70         | 80         |

TABLE VI: Limits on  $\tan\beta$  for each Higgs mass hypothesis in the maximal mixing and negative  $\mu$  scenario. For the expected limit the  $\pm 1$  and  $2\sigma$  limits are also given.

| Mass / GeV | Observed<br>limit | Expected Limits |            |        |            |            |
|------------|-------------------|-----------------|------------|--------|------------|------------|
|            |                   | $-2\sigma$      | $-1\sigma$ | Median | $+1\sigma$ | $+2\sigma$ |
| 100        | 51                | 30              | 34         | 41     | 50         | 59         |
| 110        | 49                | 28              | 32         | 39     | 46         | 54         |
| 120        | 41                | 25              | 31         | 37     | 44         | 52         |
| 130        | 32                | 26              | 31         | 36     | 44         | 52         |
| 140        | 35                | 28              | 32         | 38     | 45         | 53         |
| 150        | 36                | 29              | 33         | 40     | 47         | 55         |
| 160        | 38                | 30              | 35         | 42     | 50         | 59         |
| 170        | 46                | 34              | 39         | 45     | 54         | 64         |
| 180        | 49                | 35              | 41         | 49     | 58         | 68         |
| 190        | 57                | 38              | 45         | 53     | 63         | 74         |
| 200        | 68                | 42              | 48         | 57     | 69         | 81         |
| 220        | 89                | 47              | 57         | 68     | 82         | 95         |

TABLE VII: Limits on  $\tan\beta$  for each Higgs mass hypothesis in the no mixing and positive  $\mu$  scenario. For the expected limit the  $\pm 1$  and  $2\sigma$  limits are also given.

| Mass / GeV | Observed<br>limit | Expected Limits |            |        |            |            |
|------------|-------------------|-----------------|------------|--------|------------|------------|
|            |                   | $-2\sigma$      | $-1\sigma$ | Median | $+1\sigma$ | $+2\sigma$ |
| 100        | 48                | 28              | 33         | 40     | 47         | 55         |
| 110        | 46                | 27              | 31         | 37     | 45         | 52         |
| 120        | 39                | 26              | 30         | 36     | 43         | 51         |
| 130        | 31                | 25              | 30         | 36     | 42         | 47         |
| 140        | 34                | 26              | 31         | 37     | 44         | 52         |
| 150        | 35                | 28              | 32         | 39     | 46         | 54         |
| 160        | 37                | 30              | 34         | 41     | 49         | 56         |
| 170        | 44                | 32              | 37         | 44     | 52         | 62         |
| 180        | 47                | 34              | 40         | 47     | 56         | 65         |
| 190        | 54                | 36              | 43         | 51     | 61         | 71         |
| 200        | 64                | 39              | 46         | 55     | 65         | 77         |
| 220        | 84                | 47              | 55         | 65     | 78         | 90         |

TABLE VIII: Limits on  $\tan\beta$  for each Higgs mass hypothesis in the no mixing and negative  $\mu$  scenario. For the expected limit the  $\pm 1$  and  $2\sigma$  limits are also given.

We thank the staffs at Fermilab and collaborating institutions, and acknowledge support from the DOE and NSF (USA); CEA and CNRS/IN2P3 (France); FASI, Rosatom and RFBR (Russia); CNPq, FAPERJ, FAPESP and FUNDUNESP (Brazil); DAE and DST (India); Colciencias (Colombia); CONACyT (Mexico); KRF and KOSEF (Korea); CONICET and UBACyT (Argentina); FOM (The Netherlands); STFC and the Royal Society (United Kingdom); MSMT and GACR (Czech Republic); CRC Program, CFI, NSERC and WestGrid Project (Canada); BMBF and DFG (Germany); SFI (Ireland); The Swedish Research Council (Sweden); CAS and CNSF (China); and the Alexander von Humboldt Foundation (Germany).

- 
- [1] H.P. Nilles, Phys. Rep. **110**, 1 (1984); H.E. Haber and G.L. Kane, Phys. Rep. **117**, 75 (1985).
  - [2] S. Schael *et al.* (The ALEPH, DELPHI, L3, and OPAL Collaborations), Eur. Phys. J. C **47**, 547 (2006).
  - [3] V.M. Abazov *et al.* (D0 Collaboration), Nucl. Instrum. Methods Phys. Res. A **565**, 463 (2006).
  - [4] V.M. Abazov *et al.* (D0 Collaboration), Phys. Rev. Lett. **101**, 071804 (2008).
  - [5] D0 Collaboration, D0 Note 5740-CONF.
  - [6] V.M. Abazov *et al.* (D0 Collaboration), Phys. Rev. Lett. **101**, 221802 (2008).
  - [7] D0 Collaboration, D0 Note 5726-CONF.
  - [8] D0 Collaboration, D0 Note 5727-CONF.
  - [9] V.M. Abazov *et al.* (D0 Collaboration), Phys. Rev. Lett. **95**, 151801 (2005).
  - [10] V.M. Abazov *et al.* (D0 Collaboration), Phys. Rev. Lett. **97**, 121802 (2006).
  - [11] V.M. Abazov *et al.* (D0 Collaboration), Phys. Rev. Lett. **102**, 051804 (2009).
  - [12] A. Abulencia *et al.* (CDF Collaboration), Phys. Rev. Lett. **96**, 011802 (2006).
  - [13] CDF Collaboration, CDF Note 9071.
  - [14] CDF Collaboration, CDF Note 9284.
  - [15] G. Blazey *et al.*, arXiv:hep-ex/0005012 (2000).
  - [16] V.M. Abazov *et al.* (D0 Collaboration), Phys. Rev. Lett. **101**, 062001 (2008).
  - [17] T. Scanlon, FERMILAB-THESIS-2006-43.
  - [18] T. Sjöstrand *et al.*, arXiv:hep-ph/0308153 (2003).
  - [19] J. Pumplin *et al.*, JHEP **0207**, 012 (2002).
  - [20] J. Campbell, R.K. Ellis, F. Maltoni, and S. Willenbrock, Phys. Rev. D **67**, 095002 (2003).
  - [21] S. Jadech *et al.*, Comput. Phys. Commun. **76** (1993) 361
  - [22] E. Boos *et al.* (CompHEP Collaboration), Nucl. Instrum. Meth. A **534** (2004) 250.
  - [23] R. Brun and F. Carminati, CERN program library long writeup W5013 (1993). GEANT3 was used.
  - [24] M.L. Mangano *et al.*, JHEP **07**, 001 (2003).
  - [25] T. Junk, Nucl. Instrum. Meth. A **434** (1999) 435.; R. Barate *et al.*, Phys. Lett B **565** (2003).
  - [26] W. Fisher, FERMILAB-TM-2386-E (2007).
  - [27] S. Heinemeyer, W. Hollik, and G. Weiglein, Eur. Phys. J. C **9**, 343 (1999); Comput. Phys. Commun. **124**, 76 (2000); G. Degrossi *et al.*, Eur. Phys. J. C **28**, 133 (2003), M. Frank *et al.*, JHEP **0702**, 047 (2007). FEYNHIGGS version 2.6.3.
  - [28] M. Carena, S. Heinemeyer, C. E. M. Wagner, and G. Weiglein, Eur. Phys. J. C **45**, 797 (2006).